

Half-range lattice Boltzmann models for the simulation of Couette flow using the Shakhov collision term

Victor E. Ambruş^{a,b,*}, Victor Sofonea^a

^a*Center for Fundamental and Advanced Technical Research, Romanian Academy,
Bd. Mihai Viteazul 24, 300223 Timișoara, Romania*

^b*Department of Physics, West University of Timișoara, Bd. Vasile Pârvan 4, 300223
Timișoara, Romania*

Abstract

The three-dimensional Couette flow between parallel plates is addressed using mixed lattice Boltzmann models which implement the half-range and full-range Gauss-Hermite quadratures on the Cartesian axes perpendicular and parallel to the walls, respectively. Our models are validated through a comparison of the slip velocity results against the linearised Boltzmann equation results for values of the Knudsen number (Kn) up to 100. Furthermore, an adequate application of the Shakhov collision term allows our models to recover DSMC results for the temperature profile for Kn up to 1.0. Finally, we employ a convergence test to show that our quadrature procedure allows the simulation errors to decrease smoothly when the quadrature order is increased. We find that for low speed flows (when the non-dimensional wall velocities are ± 0.1), 108 velocities are sufficient to reduce below 1% the errors in the profiles of the particle number density, velocity, temperature and heat fluxes, from the Navier-Stokes regime (low Kn) up to the ballistic regime ($\text{Kn} \rightarrow \infty$).

Keywords: Lattice Boltzmann, Half-range Hermite polynomials, Gauss quadratures, Rarefied gases, Couette flow

1. Introduction

In the Navier-Stokes regime, it is known that the BGK approximation for the collision term is not appropriate for the realistic simulation of dissipative flows. Indeed, a Chapman-Enskog analysis shows that the Prandtl number Pr in the BGK approximation is equal to unity [1] while for hard-sphere particles, it should be equal to $2/3$. In order to achieve the correct value for Pr , we employ the Shakhov collision term [2, 3, 4, 5, 6, 7, 8], which allows Pr to be controlled as an independent quantity by modifying the thermal conductivity

*Corresponding author.

Email addresses: victor.ambrus@e-uvt.ro (Victor E. Ambruş),
sofonea@acad-tim.tm.edu.ro (Victor Sofonea)

κ_T . We will show that setting $\text{Pr} = 2/3$ through this mechanism allows the Direct Simulation Monte Carlo (DSMC) data obtained for the Couette flow of hard sphere particles [9, 10, 11, 12, 13] to be reproduced for small Kn . As Kn is increased, we find that our simulation results match the DSMC data only after adjusting the value of the Pr parameter [14].

In this paper, we only discuss the Couette flow between parallel plates. At non-negligible values of Kn , the diffuse reflection boundary conditions imposed on the plates induce a discontinuity in the distribution function [15]. For this reason, appropriate half-range quadratures should be employed on the direction perpendicular to the walls [4, 5, 6, 8, 16, 17, 18, 19, 20, 21, 22, 23, 24, 25, 26, 27, 28, 29] in order to obtain accurate results using the lattice Boltzmann (LB) method. In Ref. [28], the 2D Couette flow is simulated using mixed quadrature lattice Boltzmann models. In this paper, we extend the models in Ref. [28] to three dimensions. The ensuing models employ the half-range Gauss-Hermite quadrature on the axis perpendicular to the walls (the x axis) and the full-range Gauss-Hermite quadrature for the axes parallel to the walls (the y and z axes). The advantage of this quadrature method is described as follows. The discontinuity induced by the diffuse reflection boundary conditions imposed on the walls perpendicular to the x axis warrants the use of the half-range Gauss-Hermite quadrature, which requires $Q = N+1$ points on each Cartesian semiaxis to ensure N th order accuracy. The $2Q$ quadrature points on the whole axis are twice the number of points required by the full-range Gauss-Hermite quadrature to achieve the same degree of accuracy. Thus, it is more convenient to employ the full-range Gauss-Hermite quadratures on the y and z directions (i.e., the directions parallel to the walls), where no discontinuities in the distribution function arise, resulting in an overall smaller velocity set.

The outline of this paper is as follows. In Sec. 2, the Shakhov collision term is briefly described. Section 3 is dedicated to discussing the Boltzmann equation for the 3D Couette flow between parallel plates. Section 4 validates our models by comparing the results obtained for the slip velocity with results obtained using the linearised Boltzmann equation [30, 31]. Also, the comparison with the DSMC data of Refs. [9, 10, 11, 12, 13] is shown in this section. Section 5 discusses the convergence properties of our models with respect to the quadrature order employed for the whole spectrum of Kn . Section 6 ends this paper with conclusions. For the reader's convenience, Appendix A provides the necessary details regarding the non-dimensionalisation of the Boltzmann equation such that our simulations can be performed at the same parameters as the DSMC simulations in Ref. [13]. Finally, Appendix B presents an analysis of the number of iterations required to achieve the steady-state solution when simulating the Couette flow in the Navier-Stokes regime.

2. Boltzmann equation with the Shakhov collision term

The Boltzmann equation for a force-free flow with the Shakhov collision term [2, 3, 25, 32, 33, 34], non-dimensionalised as presented in Appendix A, reads:

$$\partial_t f + \frac{\mathbf{p}}{m} \nabla f = -\frac{1}{\tau} \left[f - f^{(\text{eq})} (1 + \mathbb{S}) \right], \quad (1)$$

where f is the Boltzmann distribution function, \mathbf{p} is the particle momentum vector, $f^{(\text{eq})}$ is the Maxwell-Boltzmann equilibrium distribution function (A.5), τ is the relaxation time given in Eq. (A.6) and \mathbb{S} is given by:

$$\mathbb{S} = \frac{1 - \text{Pr}}{nT^2} \left(\frac{\boldsymbol{\xi}^2}{5mT} - 1 \right) \mathbf{q} \cdot \boldsymbol{\xi}. \quad (2)$$

In the above, Pr gives the Prandtl number (see below), $\boldsymbol{\xi} = \mathbf{p} - m\mathbf{u}$ is the peculiar momentum, while the heat flux \mathbf{q} is obtained as a moment of f :

$$\mathbf{q} = \int d^3p \frac{\boldsymbol{\xi}^2}{2m} \frac{\boldsymbol{\xi}}{m} f. \quad (3)$$

By employing the Chapman-Enskog expansion, it can be seen that, for three-dimensional flows, the Shakhov collision term gives rise to the following expressions for the transport coefficients, namely, the dynamic (shear) viscosity η and the heat conductivity κ_T [34]:

$$\eta = \tau n T, \quad \kappa_T = \frac{1}{\text{Pr}} \frac{5}{2m} \tau n T, \quad (4)$$

where the Prandtl number Pr, calculated as

$$\text{Pr} = \frac{c_p \eta}{\kappa_T}, \quad c_p = \frac{5}{2m}, \quad (5)$$

is adjustable according to Eq. (2). The local macroscopic moments appearing above, namely, the particle number density n , the fluid velocity \mathbf{u} and the temperature T , are obtained as moments of f , as follows:

$$n = \int d^3p f, \quad (6a)$$

$$\mathbf{u} = \frac{1}{n} \int d^3p f \mathbf{p}, \quad (6b)$$

$$T = \frac{2}{3n} \int d^3p f \frac{\boldsymbol{\xi}^2}{2m}, \quad (6c)$$

while \mathbf{q} is given in Eq. (3).

3. Lattice Boltzmann models for the Couette flow

For the remainder of this paper, we shall focus on the Couette flow between parallel plates. The coordinate system is chosen such that the x axis is perpendicular to the plates, which are located at $x_{\text{left}} = -L/2$ and $x_{\text{right}} = L/2$. The plates are set in motion along the y direction with constant velocity $u_{\text{left}} = -u_w$ and $u_{\text{right}} = u_w$, while their temperature is kept constant at $T_{\text{left}} = T_{\text{right}} = T_w$.

In order to simulate the above flow, we extend the lattice Boltzmann method presented in Ref. [28] for the 2D Couette flow in the Boltzmann-BGK model to the 3D case considered here. It was shown in Ref. [28] that, for the simulation of flows at arbitrary values of Kn, the half-range Gauss-Hermite quadrature should be used on the axis perpendicular to the walls (the x axis), while a relatively low-order full-range Gauss-Hermite quadrature is adequate for the directions parallel to the walls. We shall denote the resulting models by $\text{HHLB}(Q_x) \times \text{HLB}(Q_y) \times \text{HLB}(Q_z)$, where Q_x denotes the quadrature order employed on each x semiaxis, while Q_y and Q_z denote the quadrature orders employed on the full y and z axes. The resulting velocity set comprises $2Q_x \times Q_y \times Q_z$ vectors and is the 3D extension of the 2D velocity set introduced in Refs. [28, 29].

In Ref. [28] it was shown, for a two-dimensional mixed quadrature LB model, that the value of Q_x required to obtain accurate simulation results depends on Kn and on the wall velocity u_w . Furthermore, it was also shown that, in the particular case of the BGK implementation of the collision term, the simulations employing $Q_y \geq 4$ at fixed Q_x produced identical results. In this section, a similar inequality will be determined for the quadrature orders Q_y and Q_z corresponding to the axes parallel to the walls.

Since the Couette flow is completely homogeneous along the directions which are parallel to the walls (i.e. the y and z directions), Eq. (1) reduces to:

$$\partial_t f + \frac{p_x}{m} \partial_x f = -\frac{1}{\tau} \left[f - f^{(\text{eq})} (1 + \mathbb{S}) \right], \quad (7)$$

Let us now expand f and $f^{(\text{eq})} (1 + \mathbb{S})$ with respect to the full-range Hermite polynomials on the y and z momentum axes, as follows [35]:

$$\begin{aligned} f &= \frac{\omega(\bar{p}_y)}{p_{0,y}} \frac{\omega(\bar{p}_z)}{p_{0,z}} \sum_{\ell=0}^{\infty} \frac{1}{\ell!} \sum_{s=0}^{\infty} \frac{1}{s!} \mathcal{F}_{\ell s}(x, p_x, t) H_{\ell}(\bar{p}_y) H_s(\bar{p}_z), \\ f^{(\text{eq})} (1 + \mathbb{S}) &= \frac{\omega(\bar{p}_y)}{p_{0,y}} \frac{\omega(\bar{p}_z)}{p_{0,z}} \sum_{\ell=0}^{\infty} \frac{1}{\ell!} \sum_{s=0}^{\infty} \frac{1}{s!} \mathcal{F}_{\ell s}^{\mathbb{S}}(x, p_x, t) H_{\ell}(\bar{p}_y) H_s(\bar{p}_z), \end{aligned} \quad (8)$$

where $\bar{p}_{\alpha} \equiv p_{\alpha}/p_{0,\alpha}$ ($\alpha \in \{x, y, z\}$) is the α component of the momentum vector \mathbf{p} , nondimensionalised with respect to the α component $p_{0,\alpha}$ of some reference momentum vector \mathbf{p}_0 . The weight function $\omega(x)$ for the full-range Hermite polynomials is

$$\omega(\bar{p}_{\alpha}) = \frac{1}{\sqrt{2\pi}} e^{-\bar{p}_{\alpha}^2/2}. \quad (9)$$

Furthermore, the coefficients $\mathcal{F}_{\ell s}$ and $\mathcal{F}_{\ell s}^{\mathbb{S}}$ can be computed as:

$$\begin{aligned}\mathcal{F}_{\ell s} &= \int_{-\infty}^{\infty} dp_y \int_{-\infty}^{\infty} dp_z f H_{\ell}(\bar{p}_y) H_s(\bar{p}_z), \\ \mathcal{F}_{\ell s}^{\mathbb{S}} &= \int_{-\infty}^{\infty} dp_y \int_{-\infty}^{\infty} dp_z f^{(\text{eq})} (1 + \mathbb{S}) H_{\ell}(\bar{p}_y) H_s(\bar{p}_z).\end{aligned}\quad (10)$$

The compatibility between Eqs. (8) and (10) is ensured by the orthogonality relation obeyed by the Hermite polynomials [36]:

$$\int_{-\infty}^{\infty} dx \omega(x) H_{\ell}(x) H_{\ell'}(x) = \ell! \delta_{\ell\ell'}.\quad (11)$$

Substituting Eqs. (8) into the Boltzmann equation (7) and projecting on the space of Hermite polynomials gives:

$$\partial_t \mathcal{F}_{\ell s} + \frac{p_x}{m} \partial_x \mathcal{F}_{\ell s} = -\frac{1}{\tau} (\mathcal{F}_{\ell s} - \mathcal{F}_{\ell s}^{\mathbb{S}}),\quad (12)$$

where, as before, $\mathcal{F}_{\ell s}$ and $\mathcal{F}_{\ell s}^{\mathbb{S}}$ depend on x , p_x and t . Since $f^{(\text{eq})}$ depends on n , \mathbf{u} and T , while \mathbb{S} depends on \mathbf{q} , the coefficients $\mathcal{F}_{\ell s}^{\mathbb{S}}$ always involve the coefficients $\mathcal{F}_{\ell' s'}$ of orders $0 \leq \ell' \leq 3$ and $0 \leq s' \leq 3$.¹ Thus, the Boltzmann equation (7) can be truncated at order N with respect to the Hermite basis on the p_y and p_z axes.

The order for the full-range Hermite quadratures on the y and z axes can be determined as follows. Since in this paper, only the moments of f up to \mathbf{q} are tracked, we are only interested in the evolution of the coefficients $\mathcal{F}_{\ell s}$ with $0 \leq \ell, s \leq 3$. In our implementation, we consider the expansion of $f^{(\text{eq})}$ with respect to Hermite polynomials, as follows:

$$f^{(\text{eq})} = n g_x g_y g_z,\quad (13)$$

where g_x is expanded with respect to the half-range Hermite polynomials, while g_y and g_z are expanded with respect to the full-range Hermite polynomials up to orders $N_y = Q_y - 1$ and $N_z = Q_z - 1$, respectively [28, 29]. Since \mathbb{S} is a polynomial of the third order in \mathbf{p} , the evolution of \mathbf{q} requires the recovery of the moments of $f^{(\text{eq})}$ of order $3 + 3 = 6$ on each axis. Such moments can be exactly recovered when $N_y \geq 6$ and $N_z \geq 6$, while $Q_y > N_y$ and $Q_z > N_z$.

The above analysis shows that, when the Shakhov collision term is employed, the numerical results for the 3D Couette flow considered in this paper when $Q_y, Q_z > 7$ must coincide with those obtained with $Q_y = Q_z = 7$. Therefore, we will consider the profiles obtained using the HHLB(21) \times HLB(7) \times HLB(7) model as the reference profiles which will make the subject of the following section. Afterwards, in section 5, we will consider the convergence test introduced in

¹Actually, since q_z is always 0, only the coefficients with $0 \leq s' \leq 2$ are relevant for the construction of $\mathcal{F}_{\ell s}^{\mathbb{S}}$.

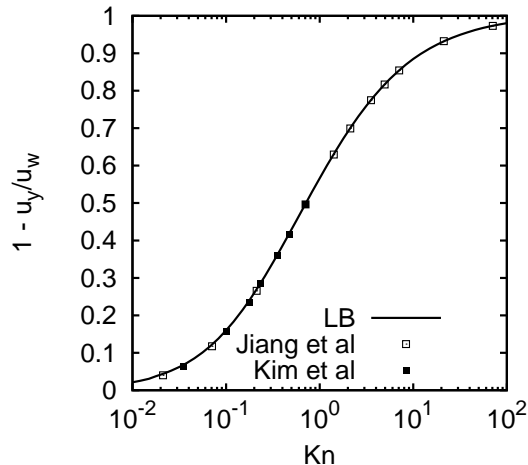


Figure 1: Comparison between the results obtained using our reference profiles and the linearised Boltzmann equation for the slip velocity. The linearised Boltzmann results are obtained from Jiang and Luo [31], as well as from Kim et al. [30] (available only up to $\text{Kn} \simeq 1$). Since the LB results do not seem to depend on the value of Pr , the plot only shows the results obtained using the BGK model (i.e. $\text{Pr} = 1.0$), for which the reference profiles were obtained using the $\text{HHLB}(21) \times \text{HLB}(4) \times \text{HLB}(4)$ model, as discussed in Sec. 3.

Refs. [28, 29] in order to determine the quadrature order required to approach the reference profile within an error of less than 1%.

Before ending this section, it is worth mentioning that if $\text{Pr} = 1$, the Shakhov term \mathbb{S} in Eq. (2) vanishes and the LB models with $Q_y, Q_z \geq 4$ give identical results, as discussed in Ref. [28].

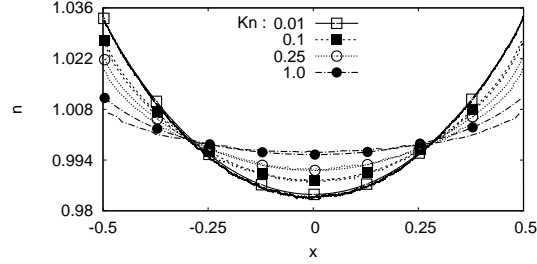
4. Reference profiles

In this section, the reference profiles obtained using the $\text{HHLB}(21) \times \text{HLB}(7) \times \text{HLB}(7)$ model are validated against the results obtained using other numerical methods. The numerical results presented in this section were obtained on a lattice of $128 \times 1 \times 1$ nodes in the x, y and z directions, respectively. The time step δt was set to 5×10^{-4} for $\text{Kn} \geq 0.1$, while for $\text{Kn} < 0.1$, the time step was decreased to $\delta t = 1 \times 10^{-4}$ in order to reduce the effect of numerical errors and to avoid the collision term becoming stiff.

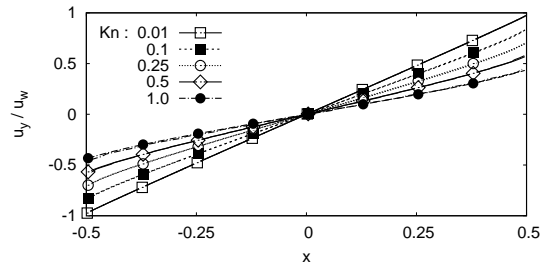
Next, we will present some information regarding the number of iterations that we performed to achieve the stationary state.

At $0.001 < \text{Kn} < 0.1$, the flow is close to the inviscid limit and an analytic analysis (see Appendix B) indicates that a number of 10^6 iterations must be performed to achieve the steady state. For large values of Kn , the ballistic

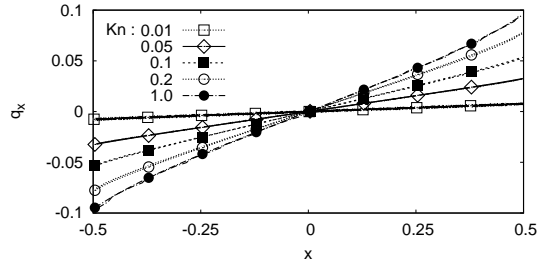
Kn :



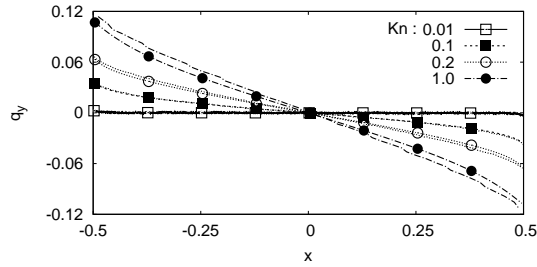
(a)



(b)



(c)



(d)

Figure 2: Reference profiles of the (a) density n , (b) normalised longitudinal velocity u_y/u_w , (c) transverse heat flux q_x and (d) longitudinal heat flux q_y , obtained using the HHLB(21) \times HLB(7) \times HLB(7) model, corresponding to the Couette flow between parallel plates at temperature $T_w = 1.0$ and velocity $u_w = 0.63$. The LB results (lines and points) for various values of the Knudsen number Kn are compared to the corresponding DSMC results (lines only) presented in Ref. [9]. The same type of line is used to plot both the LB and the DSMC results for each Kn .

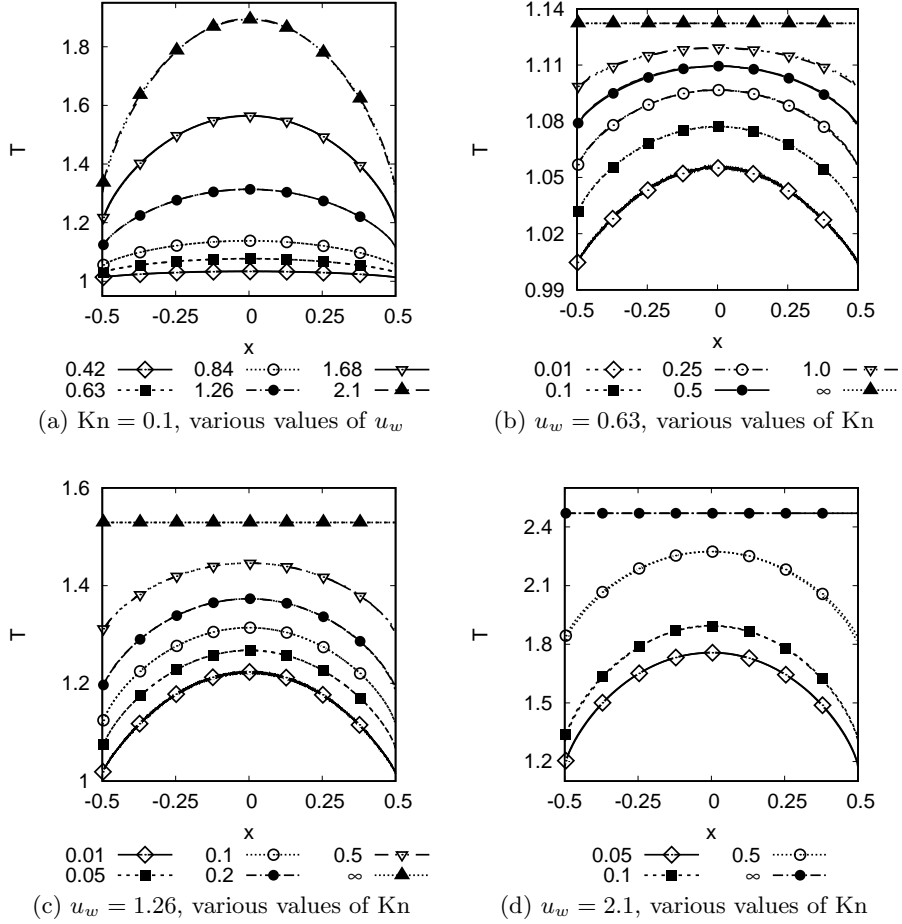


Figure 3: Comparison between the temperature profiles obtained using the HHLB(21) \times HLB(7) \times HLB(7) model (lines and points) and the DSMC results (lines) reported in Ref. [13]: (a) $Kn = 0.1$ and various values of the plate velocity u_w ; (b) $u_w = 0.63$ and various values of Kn ; (c) same, with $u_w = 1.26$; (d) same, with $u_w = 2.1$. In (b), (c) and (d), the LB results obtained in the ballistic limit are compared with the analytic result (15).

regime sets in, where the time scale on which the flow becomes stationary is that required by the particles in the initial state to reach the boundary walls. For a quadrature order $Q_x = 21$, the slowest particle has $p_x \simeq 0.0188$, requiring a time $\Delta t \simeq 53.2$ to cross the unit-length channel. Since $\delta t = 5 \times 10^{-4}$, a number of $\sim 106,383$ iterations are required for this particle to cross the channel. Thus, for all $\text{Kn} \geq 1$, we always performed 200,000 iterations.

When $0.1 \leq \text{Kn} < 1.0$, the flow is neither in the inviscid regime nor in the ballistic regime. At $\text{Kn} = 0.1$, Eq. (B.12) implies that a number of 10,000 iterations should suffice to achieve the steady state. We found that, for the above range of Kn , 60,000 iterations were sufficient for the flow to become stationary.

For the spatial advection, we employed the second order flux limiter scheme described in Refs. [28, 29], while the time stepping was performed using a third-order Runge-Kutta algorithm [37]. The implementation of the diffuse reflection boundary conditions on the channel walls is identical to that presented in Refs. [28, 29].

In Figure 1, we present a comparison between the results obtained using our reference model and those obtained using the linearised Boltzmann equation in Refs. [30], as well as the benchmark results published in Ref. [31], for the velocity slip u_{slip} , defined as follows:

$$u_{\text{slip}} = u_w - u(x = L/2). \quad (14)$$

In order to compare with the results in Ref. [30], the Knudsen number introduced therein was multiplied by a factor of $\sqrt{2/\pi}$, i.e. $\text{Kn} \rightarrow \text{Kn}\sqrt{2/\pi}$. Similarly, the Knudsen number employed in Ref. [31] was rescaled using a factor of $1/\sqrt{2}$. The above rescaling of Kn is necessary because of the various conventions used to relate this dimensionless number to the relaxation time τ .

The results presented in Fig. 1 were obtained for $u_w = 0.1$. At higher values of u_w , the LB results present slight deviations from the benchmark results. This is to be expected, since the profile of u_y/u_w does not scale perfectly with u_w , as also demonstrated in Ref. [38]. It is remarkable that the velocity profiles obtained using our models do not seem to depend on the value of Pr . In particular, the BGK collision term and the Shakhov collision term with $\text{Pr} = 2/3$ and with $\text{Pr} = 4/3$ yield identical results. It can be seen that the agreement between our results and those reported in Refs. [30, 31] is very good.

Next, we considered a comparison against the Direct Simulation Monte Carlo (DSMC) results reported in [13], and also in Refs. [9, 10, 11, 12]. The correspondence between our simulation parameters and the quantities employed in the DSMC simulations was taken into account in the non-dimensionalisation procedure, which we discuss in Appendix A.

Fig. 2 shows a comparison between our reference profiles and the DSMC profiles obtained for the number density n (a), velocity parallel to the walls u_y (b), as well as for the transversal q_x (c) and longitudinal q_y (d) heat fluxes. Our convention is that the LB results are shown using lines and points, while the corresponding DSMC results are shown for comparison with the same line

type, but without points. Despite some visible discrepancies at large Kn in the profiles of n and q_y , the agreement between our simulation results and the DSMC results is excellent, especially for u_y and q_x , where the DSMC and LB results are almost everywhere overlapped. While the profiles of u_y and q_x seem to be independent of the value of Pr, n and q_y are not. The values of Pr at which the presented results were obtained were chosen to match the DSMC results for the temperature profile, as discussed in the following paragraph.

The temperature profiles obtained using our reference LB model are compared with the DSMC results of Ref. [13] in Fig. 3. In plot (a), the temperature profiles at Kn = 0.1 for various values of u_w are shown. The agreement between the LB (lines and points) and the DSMC (lines) results is excellent. Here, the Prandtl number was set to Pr = 0.67 for $u_w = 0.42$, to Pr = 0.685 at $u_w = 0.63$, while at $u_w = 0.84, 1.26, 1.68$ and 2.1 , we found that a good fit of the LB results to the DSMC data was obtained at Pr = 0.695. In plot (b), the wall velocity is fixed at $u_w = 0.63$ for various values of Kn. We used the following pairs of values (Kn, Pr) $\in \{(0.01, 0.67), (0.1, 0.685), (0.25, 0.78), (0.5, 0.9), (1.0, 1.2)\}$. Also represented in this plot is the result in the ballistic regime, where [22]:

$$T_{\text{ballistic}} = \sqrt{T_+ T_-} \left[1 + \frac{4mu_w^2}{3(\sqrt{T_+} + \sqrt{T_-})^2} \right], \quad (15)$$

which reduces to $T_{\text{ballistic}} = T_w + mu_w^2/3$ in the case when the plates have equal temperature. The observed agreement is excellent. In plot (c) the wall velocity is taken to be $u_w = 1.26$. The good agreement observed in this case was obtained using (Kn, Pr) $\in \{(0.01, 0.67), (0.05, 0.67), (0.25, 0.785), (0.5, 0.98)\}$. Finally, (d) shows the case when $u_w = 2.1$, for which the following values were used: (Kn, Pr) $\in \{(0.05, 0.67), (0.1, 0.695), (0.25, 0.785), (0.5, 1.145)\}$.

5. Convergence tests

In order to assess the computational demand for a given level of accuracy while using the mixed lattice Boltzmann models employed in this paper, we perform the convergence test described in Refs. [28, 29]. Before discussing the results, let us briefly summarise the procedure employed for this test.

The convergence test is performed by comparing the macroscopic profiles $M \in \{n, u_y, T, q_x, q_y\}$ obtained with a given model and corresponding reference profiles M_{ref} obtained using a high-order model. Defining the error for the profile M as:

$$\varepsilon_M = \frac{\max_x [|M(x) - M_{\text{ref}}(x)|]}{\Delta M}, \quad (16)$$

where $\Delta M = \min\{\max_x [M_{\text{ref}}(x)] - \min_x [M_{\text{ref}}(x)], 0.1\}$, a model is considered to have achieved convergence when the maximum error

$$\varepsilon = \max_M \varepsilon_M \quad (17)$$

satisfies the following criterion:

$$\varepsilon < 0.01. \quad (18)$$

We have performed the above convergence test for $0.01 \leq \text{Kn} \leq 10^4$ by using a logarithmic scale with twelve points per factor of 10 (i.e. the points 1, 1.2, 1.5, 1.8, 2.2, 2.6, 3.2, 3.8, 4.6, 5.6, 6.8, 8.3, 10 were used between 1 and 10). In our tests we have used three values for Pr and two values for the wall velocities u_w , namely $\text{Pr} \in \{\frac{2}{3}, 1, \frac{4}{3}\}$ and $u_w \in \{0.1, 1.0\}$. The reference profiles were obtained using the HHLB(21) \times HLB(7) \times HLB(7) model, except in the BGK case (when Pr = 1), when the model used for the reference profiles was chosen to be HHLB(21) \times HLB(4) \times HLB(4), as discussed in Sec. 3. Our strategy for this convergence test was to construct the profiles relevant to the convergence test (18) using all models of type HHLB(Q_x) \times HLB(Q_y) \times HLB(Q_z), where $1 \leq Q_x \leq 21$, while Q_y and Q_z were taken to have equal value given by the minimum between Q_x and either 4 in the BGK case, or 6 when Pr \neq 1, as follows²:

$$Q_y = Q_z = \begin{cases} \min(Q_x, 4) & \text{Pr} = 1.0, \\ \min(Q_x, 6) & \text{Pr} \neq 1.0. \end{cases} \quad (19)$$

The results of the convergence test (18) are summarised in Fig. 4. In these plots, the horizontal axis represents Kn in logarithmic scale, while the vertical axis represents the quadrature order Q_{conv} on the x axis (corresponding to the half-range Gauss-Hermite quadrature) required for convergence. It is interesting to see that, for fixed u_w , Q_{conv} does not vary significantly with Pr. The visible differences occur only at large wall velocities ($u_w = 1.0$), where, at small Kn, the recovery of the Navier-Stokes regime requires $Q_y = Q_z = 6$ for the Shakhov collision term, while $Q_y = Q_z = 4$ is sufficient when the BGK case is implemented. It can also be seen that, at fixed Pr and Kn, Q_{conv} increases as u_w is increased.

For the case when $u = 0.1$, a relatively small velocity set is required to obtain accurate results throughout the whole spectrum of Kn. Indeed, the model HHLB(6) \times HLB(6) \times HLB(6), which employs a number of $2 \times 6^3 = 432$ velocities, is sufficient to satisfy the 1% convergence test of Eq. (18), as can be seen from Fig. 4(a). In fact, for this flow regime, the quadrature orders on the y and z axes can be further reduced to $Q_y = Q_z = 3$, such that the convergence test is satisfied throughout the Kn range with the model HHLB(6) \times HLB(3) \times HLB(3), which employs only 108 velocities.

²Note that the analysis in Sec. 3 indicated that the Q_y and Q_z should be set to 7 in order to recover the evolution of the heat flux. However, our numerical experiments have demonstrated that the results obtained using $Q_y = Q_z = 6$ are essentially identical to those corresponding to $Q_y = Q_z = 7$, as long as Q_x is sufficiently large.

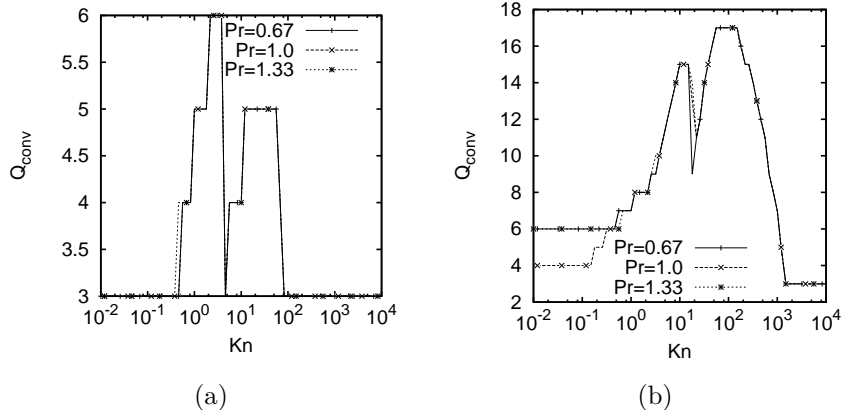


Figure 4: Quadrature order Q_{conv} on the x axis required to satisfy the convergence test (18) for (a) $u_w = 0.1$ and (b) $u_w = 1.0$.

6. Conclusion

In this paper, we have extended the mixed quadrature lattice Boltzmann models introduced in Ref. [28] to the case of a 3D Couette flow, for the simulation of which we employed the half-range Gauss-Hermite quadrature on the axis perpendicular to the walls and the full-range Gauss-Hermite quadrature on the two axes which are parallel to the walls.

We first validated our models by comparing the value of the slip velocity obtained for values of the Knudsen number Kn between 0.01 and 100 with the benchmark solution of Ref. [31], as well as with the linearised Boltzmann results reported in Ref. [30]. Furthermore, we compared the particle number density, velocity, temperature and heat flux profiles with the Direct Simulation Monte Carlo (DSMC) results reported in Refs. [9, 10, 11, 12, 13]. Here, we found that the hard-sphere results could be successfully recovered by employing the Shakhov collision term, which allows the Prandtl number Pr to be modified. While at small values of the Knudsen number Kn , the value of Pr for hard-sphere particles is $2/3$, the value of Pr at higher Kn had to be adjusted to fit the DSMC data. In general, we observed good agreement with all of the above data.

Finally, we performed a convergence test with respect to the quadrature order (i.e. the number of velocities). We found that our models can be used to obtain accurate results throughout the whole Kn range (i.e. ranging from the Navier-Stokes regime at $\text{Kn} = 10^{-3}$ up to the ballistic regime). For low-speed flows (i.e. $u_w = 0.1$, corresponding to ~ 23.81 m/s), the $\text{HHLB}(6) \times \text{HLB}(3) \times \text{HLB}(3)$ model (employing $12 \times 3 \times 3 = 108$ velocities) can be used to obtain results which have errors of less than 1% in the profiles of n , u_y , T , q_x and q_y .

when compared to the reference profiles. In the case when $u_w = 1.0$, errors less than 1% are ensured by the HHLB(17) \times HLB(6) \times HLB(6) model, which employs 1224 velocities.

Acknowledgements

This work was supported by a grant of the Romanian National Authority for Scientific Research, CNCS-UEFISCDI, Project No. PN-II-ID-PCE-2011-3-0516. The authors express their gratitude to Prof. Henning Struchtrup (Department of Mechanical Engineering, University of Victoria, Canada) for kindly providing the DSMC results used for the validation of our models.

Appendix A. Non-dimensionalisation of the Boltzmann equation

In order to run our simulations using the same parameters as in the DSMC simulations reported in Ref. [13], the Boltzmann equation was nondimensionalised as follows. In this section, we employ the convention that the quantities before nondimensionalisation are denoted using a tilde $\tilde{\cdot}$. The reference temperature was taken to be $\tilde{T}_{\text{ref}} = 273$ K. Since Ref. [13] used Argon gas atoms in their simulations, we chose the reference mass to be equal to $\tilde{m}_{\text{ref}} = \tilde{m}_{\text{Ar}} \simeq 6.63 \times 10^{-26}$ kg. The resulting reference velocity is:

$$\tilde{c}_{\text{ref}} = \sqrt{\frac{\tilde{k}_B \tilde{T}_{\text{ref}}}{\tilde{m}_{\text{ref}}}} \simeq 238.35 \frac{\text{m}}{\text{s}}, \quad (\text{A.1})$$

where the Boltzmann constant \tilde{k}_B also has a tilde since it is not dimensionless. The average particle number density was taken to be $\tilde{n} = 1.4 \times 10^{20}$ molecules/m³, while the mean free path was chosen as $\tilde{\lambda} = 0.008833$ m. The Knudsen number Kn was controlled by varying the domain size, such that the reference length, reference time and reference densities depend on Kn, as shown in Table A.1.

The non-dimensional form of the Boltzmann equation can be achieved starting from the Boltzmann equation:

$$\partial_t \tilde{f} + \frac{\tilde{\mathbf{p}}}{\tilde{m}} \tilde{\nabla} \tilde{f} = -\frac{1}{\tilde{\tau}} (\tilde{f} + \tilde{f}^{(\text{eq})}). \quad (\text{A.2})$$

First, the non-dimensional distribution function f is defined as:

$$f = \frac{\tilde{f}}{\tilde{n}_{\text{ref}}} (\tilde{m}_{\text{ref}} \tilde{k}_B \tilde{T}_{\text{ref}})^{3/2}, \quad (\text{A.3})$$

In the case of the Maxwell-Boltzmann distribution,

$$\tilde{f}^{(\text{eq})} = \frac{\tilde{n}}{(2\pi \tilde{m} \tilde{k}_B \tilde{T})^{3/2}} \exp \left[-\frac{(\tilde{\mathbf{p}} - \tilde{m} \tilde{\mathbf{u}})^2}{2\tilde{m} \tilde{k}_B \tilde{T}} \right], \quad (\text{A.4})$$

	l_{ref}	t_{ref}	n_{ref}
Kn = 0.01	0.8833 m	3.71 ms	1.24×10^{20} molecules/m ³
Kn = 0.05	0.17666 m	0.741 ms	2.47×10^{19} molecules/m ³
Kn = 0.1	0.08833 m	0.371 ms	1.24×10^{19} molecules/m ³
Kn = 0.25	0.035332 m	0.148 ms	4.95×10^{18} molecules/m ³
Kn = 0.5	0.017666 m	74.1 μ s	2.47×10^{18} molecules/m ³
Kn = 1.0	0.008833 m	37.1 μ s	1.24×10^{18} molecules/m ³

Table A.1: Reference values for the length, time and density for various values of Kn.

this procedure yields:

$$f^{(\text{eq})} = \frac{n}{(2\pi mT)^{3/2}} \exp \left[-\frac{(\mathbf{p} - m\mathbf{u})^2}{2mT} \right], \quad (\text{A.5})$$

where $\mathbf{p} \equiv \tilde{\mathbf{p}}/\tilde{m}_{\text{ref}}\tilde{c}_{\text{ref}}$. Finally, the Boltzmann equation (A.2) can be non-dimensionalised after multiplying both sides by $\tilde{t}_{\text{ref}}(\tilde{m}_{\text{ref}}\tilde{k}_B\tilde{T}_{\text{ref}})^{3/2}/\tilde{n}_{\text{ref}}$, yielding Eq. (1). The non-dimensionalised relaxation time τ has the following form [39]:

$$\tau = \frac{\text{Kn}}{n}. \quad (\text{A.6})$$

Appendix B. Velocity relaxation in the hydrodynamic limit of the Couette flow

The Navier-Stokes equation reads:

$$\rho[\partial_t \mathbf{u} + (\mathbf{u} \cdot \nabla)\mathbf{u}] = -\nabla P + \frac{1}{3}\eta\nabla(\nabla\mathbf{u}) + \eta\Delta\mathbf{u}, \quad (\text{B.1})$$

where a vanishing bulk viscosity and a constant coefficient of shear viscosity μ were considered. To obtain an approximation of the evolution of u_y in the case of the Couette flow, let us consider the case of small wall velocities $\pm u_w$, such that the flow is close to isothermal and incompressible. Thus, $\nabla\mathbf{u} \simeq 0$ and $P = nT$ is constant throughout the channel, such that Eq. (B.1) reduces to:

$$\frac{\partial u_y}{\partial t} - \frac{\eta}{\rho} \frac{\partial^2 u_y}{\partial x^2} = 0. \quad (\text{B.2})$$

The boundary conditions $u(x = \pm L/2) = \pm u_w$ can be satisfied by considering:

$$u_y(x, t) = \frac{2u_w x}{L} + \tilde{u}_y(x, t), \quad (\text{B.3})$$

where $\tilde{u}_y(x = \pm L/2, t) = 0$. Writing $\tilde{u}_y = e^{-\lambda t} U_\lambda(x)$ gives:

$$\frac{\partial^2 U_\lambda}{\partial x^2} + \frac{\rho\lambda}{\eta} U_\lambda = 0. \quad (\text{B.4})$$

The solution of the above equation is:

$$U_\lambda(x) = A_\lambda \cos\left(x\sqrt{\rho\lambda/\eta}\right) + B_\lambda \sin\left(x\sqrt{\rho\lambda/\eta}\right). \quad (\text{B.5})$$

Assuming that the solution is antisymmetric gives $A_\lambda = 0$, while the parameter λ is constrained such that the sine function vanishes at $x = \pm L/2$:

$$\lambda \rightarrow \lambda_k = \frac{4k^2\pi^2\eta}{\rho L^2}. \quad (\text{B.6})$$

Thus, the solution of Eq. (B.2) is [40]:

$$u_y = \frac{2u_w x}{L} + \sum_{k=1}^{\infty} e^{-\lambda_k t} a_k \sin \frac{2k\pi x}{L}. \quad (\text{B.7})$$

The coefficients a_k can be obtained by requiring that $u_y(x, t = 0) = 0$ (our initial state for this problem):

$$a_k = -\frac{2}{L} \int_{-L/2}^{L/2} dx \frac{2u_w x}{L} \sin \frac{2k\pi x}{L} = \frac{2u_w}{\pi k} (-1)^k. \quad (\text{B.8})$$

The following solution is obtained:

$$u_y(x, t) = u_y^{\text{st}}(x) + u_y^t(x, t), \quad (\text{B.9a})$$

where the stationary state solution is $u_y^{\text{st}} = 2u_w x/L$ and the transient part u_y^t is:

$$u_y^t = \frac{2u_w}{\pi} \sum_{k=1}^{\infty} \frac{(-1)^k}{k} e^{-\lambda_k t} \sin \frac{2k\pi x}{L}. \quad (\text{B.9b})$$

Let us estimate the time $t_{1\%}$ required for u_y^t (B.9b) to decay to less than 1% of u_w . As $t \rightarrow \infty$, the leading order term $e^{-\lambda_1 t}$ dominates. Requiring that $|a_1|e^{-\lambda_1 t_{1\%}} = 0.01u_w$, where $a_1 = -\frac{2u_w}{\pi}$ (B.8), gives:

$$t_{1\%} \simeq \frac{4.154}{\lambda_1}. \quad (\text{B.10})$$

The coefficient λ_1 is given by:

$$\lambda_1 = \frac{4\pi^2\eta}{\rho L^2}. \quad (\text{B.11})$$

In our simulations, $\rho \simeq 1$, $L = 1$ and $\eta = \tau n T \simeq \text{Kn}$, such that $\lambda_1 \simeq 4\pi^2 \text{Kn}$. With this approximation, we obtain

$$t_{1\%} \simeq \frac{0.105}{\text{Kn}}. \quad (\text{B.12})$$

In the case when $\text{Kn} = 10^{-3}$ the damping time $t_{1\%} \simeq 105$. Since in this regime, we used $\delta t = 10^{-4}$ per time step, the number of iterations required to achieve $t = t_{1\%}$ is

$$N_{\text{iter}} \simeq 1.05 \times 10^6. \quad (\text{B.13})$$

References

References

- [1] C. Cercignani, *The Boltzmann Equation and Its Applications*, Springer-Verlag, New York, 1988.
- [2] E. M. Shakhov, Generalization of the krook kinetic relaxation equation, *Fluid Dyn.* 3 (1968) 95–96. doi:10.1007/BF01029546.
- [3] E. M. Shakhov, Approximate kinetic equations in rarefied gas theory, *Fluid Dyn.* 3 (1968) 112–115. doi:10.1007/BF01016254.
- [4] J. Y. Yang, J. C. Huang, L. Tsuei, Numerical solutions of the nonlinear model Boltzmann equations, *Proc. R. Soc. Lond. A* 448 (1995) 55–80. doi:10.1098/rspa.1995.0003.
- [5] Z.-H. Li, H.-X. Zhang, Numerical investigation from rarefied flow to continuum by solving the boltzmann model equation, *Int. J. Numer. Meth. Fluids* 42 (2003) 361–382. doi:10.1002/flid.517.
- [6] Z.-H. Li, H.-X. Zhang, Study on gas kinetic unified algorithm for flows from rarefied transition to continuum, *J. Comput. Phys* 193 (2004) 708–738. doi:10.1016/j.jcp.2003.08.022.
- [7] Z.-H. Li, H.-X. Zhang, S. Fu, Gas kinetic algorithm for flows in Poiseuille-like microchannels using Boltzmann model equation, *Science in China Ser. G* 48 (2005) 496–512. doi:10.1360/04yw0106.
- [8] Z.-H. Li, H.-X. Zhang, Gas-kinetic numerical studies of three-dimensional complex flows on spacecraft re-entry, *J. Comput. Phys* 228 (2009) 1116–1138. doi:10.1016/j.jcp.2008.10.013.
- [9] H. Struchtrup, M. Torrilhon, H theorem, regularization, and boundary conditions for linearized 13 moment equations, *Phys. Rev. Lett.* 99 (2007) 014502. doi:10.1103/PhysRevLett.99.014502.
- [10] H. Struchtrup, M. Torrilhon, Higher-order effects in rarefied channel flows, *Phys. Rev. E* 78 (2008) 046301. doi:10.1103/PhysRevE.78.046301.
- [11] M. Torrilhon, H. Struchtrup, Boundary conditions for regularized 13-moment-equations for micro-channel-flows, *J. Comput. Phys.* 227 (2008) 1982–2011. doi:10.1016/j.jcp.2007.10.006.
- [12] P. Taheri, M. Torrilhon, H. Struchtrup, Couette and Poiseuille microflows: Analytical solutions for regularized 13-moment equations, *Phys. Fluids* 21 (2009) 017102. doi:10.1063/1.3064123.
- [13] A. Schuetze, *Direct Simulation by Monte Carlo modeling Couette flow using dsmclas.f: A user’s manual* (Report, Department of Mechanical Engineering, University of Victoria, Canada) (2003).

- [14] Z. Guo, Application of discrete unified gas kinetic scheme for temperature induced non-equilibrium flows, the Thirteenth International Conference for Mesoscopic Methods in Engineering and Science ICMMES-2016 (2016).
URL https://www.conftool.net/icmmes2016/index.php?page=browseSessions&form_session=48#p
- [15] E. P. Gross, E. A. Jackson, S. Ziering, Boundary value problems in kinetic theory of gases, *Ann. Phys.* 1 (1957) 141–167. doi:10.1016/0003-4916(57)90056-8.
- [16] S. Lorenzani, L. Gibelli, A. Frezzotti, A. Frangi, C. Cercignani, Kinetic approach to gas flows in microchannels, *Nanoscale and Microscale Thermophysical Engineering* 11 (2007) 211–226. doi:10.1080/15567260701333489.
- [17] A. Frezzotti, L. Gibelli, B. Franzelli, A moment method for low speed microflows, *Continuum Mech. Thermodyn.* 21 (2009) 495–509. doi:10.1007/s00161-009-0128-y.
- [18] A. Frezzotti, G. P. Ghiroldi, L. Gibelli, Solving the Boltzmann equation on GPUs, *Comput. Phys. Comm.* 182 (2011) 2445–2453. doi:10.1016/j.cpc.2011.07.002.
- [19] L. Gibelli, Velocity slip coefficients based on the hard-sphere Boltzmann equation, *Phys. Fluids* 24 (2012) 022001. doi:10.1063/1.3680873.
- [20] Z. Guo, K. Xu, R. Wang, Discrete unified gas kinetic scheme for all Knudsen number flows: Low-speed isothermal case, *Phys. Rev. E* 88 (2013) 033305. doi:10.1103/PhysRevE.88.033305.
- [21] G. P. Ghiroldi, L. Gibelli, A direct method for the Boltzmann equation based on a pseudo-spectral velocity space discretization, *J. Comput. Phys.* 258 (2014) 568–584. doi:10.1016/j.jcp.2013.10.055.
- [22] V. E. Ambruş, V. Sofonea, Implementation of diffuse-reflection boundary conditions using lattice Boltzmann models based on half-space Gauss-Laguerre quadratures, *Phys. Rev. E* 89 (2014) 041301(R). doi:10.1103/PhysRevE.89.041301.
- [23] V. E. Ambruş, V. Sofonea, Application of lattice Boltzmann models based on Laguerre quadratures in complex flows, *Interfac. Phenom. Heat Transfer* 2 (2014) 235–251. doi:10.1615/InterfacPhenomHeatTransfer.2015011655.
- [24] V. E. Ambruş, V. Sofonea, Lattice Boltzmann models based on Gauss quadratures, *Int. J. Mod. Phys. C* 25 (2014) 1441011. doi:10.1142/S0129183114410113.
- [25] Z. Guo, , R. Wang, K. Xu, Discrete unified gas kinetic scheme for all knudsen number flows. ii. thermal compressible case, *Phys. Rev. E* 91 (2015) 033313. doi:10.1103/PhysRevE.91.033313.

- [26] G. P. Ghiroldi, L. Gibelli, A finite-difference lattice Boltzmann approach for gas microflows, *Commun. Comput. Phys.* 17 (2015) 1007–1018. doi:10.4208/cicp.2014.m424.
- [27] Y. Shi, Y. W. Yap, J. E. Sader, Linearized lattice Boltzmann method for micro- and nanoscale flow and heat transfer, *Phys. Rev. E* 92 (2015) 013307. doi:10.1103/PhysRevE.92.013307.
- [28] V. E. Ambruş, V. Sofonea, Lattice Boltzmann models based on half-range Gauss-Hermite quadratures, *J. Comput. Phys.* 316 (2016) 760–788. doi:10.1016/j.jcp.2016.04.010.
- [29] V. E. Ambruş, V. Sofonea, Application of mixed quadrature lattice Boltzmann models for the simulation of Poiseuille flow at non-negligible values of the Knudsen number, *J. Comput. Sci.* 17 (2016) 403–417. doi:10.1016/j.jocs.2016.03.016.
- [30] S. H. Kim, H. Pitsch, I. D. Boyd, Accuracy of higher-order lattice Boltzmann methods for microscale flows with finite Knudsen numbers, *J. Comput. Phys.* 227 (2008) 8655–8671. doi:10.1016/j.jcp.2008.06.012.
- [31] S. Jiang, L.-S. Luo, Analysis and accurate numerical solutions of the integral equation derived from the linearized BGKW equation for the steady Couette flow, *J. Comput. Phys* 316 (2016) 416–434. doi:10.1016/j.jcp.2016.04.011.
- [32] V. A. Titarev, Conservative numerical methods for model kinetic equations, *Comput. Fluids* 36 (2007) 1446–1459. doi:10.1016/j.compfluid.2007.01.009.
- [33] I. A. Graur, A. P. Polikarpov, Comparison of different kinetic models for the heat transfer problem, *Heat Mass Transf.* 46 (2009) 237–244. doi:10.1007/s00231-009-0558-x.
- [34] V. E. Ambruş, V. Sofonea, High-order thermal lattice Boltzmann models derived by means of Gauss quadrature in the spherical coordinate system, *Phys. Rev. E* 86 (2012) 016708. doi:10.1103/PhysRevE.86.016708.
- [35] F. B. Hildebrand, *Introduction to Numerical Analysis*, second edition Edition, Dover Publications, 1987.
- [36] F. W. J. Olver, D. W. Lozier, R. F. Boisvert, C. W. Clark, *NIST Handbook of Mathematical Functions*, Cambridge University Press, New York, 2010.
- [37] S. Gottlieb, C.-W. Shu, Total variation diminishing runge-kutta schemes, *Math. Comput.* 67 (1998) 73–85. doi:10.1090/S0025-5718-98-00913-2.
- [38] O. Rogozin, Numerical analysis of the nonlinear plane Couette-flow problem of a rarefied gas for hard-sphere molecules, *Eur. J. Mech. B-Fluid* 60 (2016) 148–163. doi:10.1016/j.euromechflu.2016.06.011.

- [39] Y. Sone, *Molecular Gas Dynamics: Theory, Techniques and Applications*, Birkhäuser, Boston, 2007.
- [40] C. Pozrikidis, *Introduction to Theoretical and Computational Fluid Dynamics*, Oxford University Press, Oxford, 1997.